Hydrothermal Synthesis of Potassium Hexatitanates under Subcritical and Supercritical Water Conditions and Its Application in Photocatalysis

Rosiyah Binti Yahya,† Hiromichi Hayashi,* Takako Nagase, Takeo Ebina, Yoshio Onodera, and Norio Saitoh

Tohoku National Industrial Research Institute, Nigatake 4-2-1, Miyagino-ku, Sendai, 983-8551, Japan

Received July 10, 2000. Revised Manuscript Received November 16, 2000

Hydrothermal synthesis of potassium hexatitanate was carried out under various subcritical and supercritical water conditions using potassium hydroxide and titanium tetraisopropoxide as starting materials. Characterization of these hydrothermally synthesized potassium hexatitanates by XRD, SEM, TEM, and thermal analysis showed that long, felted-like fibers of potassium hexatitanates were formed and these fibers are thermally stable up to 1273 K. The use of these fibers as photocatalysts in water decomposition was investigated using ruthenium oxide as the catalytic active phase. Photocatalytic activitiy in the water decomposition reaction was found to be much higher in comparison with the solid state synthesized photocatalyst. Activites of more than 13-fold were obtained for the photocatalysts synthesized under subcritical water conditions and between 27- and 59-fold for those synthesized under supercritical water conditions for water decomposition.

Introduction

Potassium hexatitanate is among the materials that has attracted growing interest due to its potential economic importance. This relatively cheap fibrous material has thermal durability, chemical resistivity, and dispersibility and has found its use as reinforcing material for plastics, heat-insulating paints, and filter materials.[1,2] The structure of this material is one in which the octahedral TiO_6 share an edge at one level in a linear groups of three, giving rise to a rectangular tunnel structure (Figure 1).[3] This tunnel structure has also attracted additional interest in its application as photocatalytic materials. Alkali-metal haxatitanate is one of the semiconducting photocatalysts which has the capability of invoking a photocatalytic decomposition of water to produce H_2 and O_2.[4−7] Inoue et al. has reported that alkali-metal hexatitanate when incorporated with noble metal oxides exhibited noticeable photocatalytic activity in the decomposition of water.[4] The presence of these tunnels in the structure has the advantage of being able to accommodate the active phase, which acts as a promoter,[8] thus enhancing further the catalytic activity.

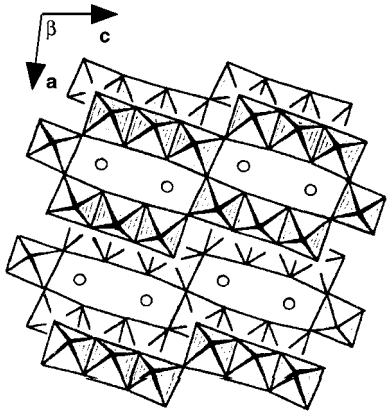

Figure 1. Structure of potassium hexatitanate—the corners join adjacent sheets to form a framework enclosing tunnels with two potassium ions in each tunnel.

The varied applications of this material have somehow demanded material scientists to find a suitable and efficient method of synthesis with improved physical and structural properties. Berry et al. reported that potassium hexatitanate fibers could be obtained from the K_2O-TiO_2 system in supercritical water or molten KCl and from K_2O-TiO_2–KF melt systems in molten KCl.[9] Giez et al. found that the hydrothermal reaction of alkali-metal hydroxide and titanium dioxide at 873−973 K under 500−4000 atm could also produce fibrous potassium hexatitantes.[10] The flux evaporation method using nonfibrous potassium hexatitanate (prepared from

† Department of Chemistry, Faculty of Science, University of Malaya, 50603 Kuala Lumpur, Malaysia.

(1) Richardson, M. O. *Polymer Engineering Composites*; International Ideas: Philadelphia, 1977.
(2) Gulledge, H. C. *Ind. Eng. Chem.* **1960**, *52*, 117.
(3) Andersson, S.; Wadsley, A. D. *Acta Crystallogr.* **1962**, *15*, 194.
(4) Inoue, Y.; Kubokawa, T.; Sato, K. *J. Phys. Chem.* **1991**, *95*, 4059.
(5) Kudo, A.; Tanaka, A.; Domen, K.; Maruya, K.; Akita, K.; Onishi, T. *J. Catal.* **1988**, *111*, 67.
(6) Tanaka, T.; Furumi, Y.; Shinohara, K.; Tanaka, A.; Hara, M.; Kondo, J. N.; Domen, K. *Chem. Mater.* **1997**, *9*, 1063.
(7) Ebina, Y.; Tanaka, A.; Kondo, J. N.; Domen, K. *Chem. Mater.* **1996**, *8*, 2534.
(8) Ogura, S.; Kohno, M.; Sato, K.; Inoue, Y. *Phys. Chem. Chem. Phys.* **1999**, *1*, 179.
(9) Berry, K. L.; Aftandilian, V. D.; Gilbert, W. W.; Meibohm, E. P. H.; Young, H. S. *J. Inorg. Nucl. Chem.* **1960**, *14*, 231.
(10) Salzberg, P. L.; Gier, T. E.; Young, H. S. US Patent 2,833,620, 1958.

10.1021/cm000561p CCC: $20.00
Published on Web 01/31/2001

Table 1. Analytical Data and Crystalline Size Values in the Direction of (200) Reflection[a]

sample	heating temp, K	heating duration, h	pressure, MPa	Ru loading, wt %	surface area, m^2/g	pore vol, cm^3/g	*L* (200), nm
S1 (sub)	623	2	14.2	0.27	83	0.27	13.4
S2 (sub)	623	5	16.2	0.26	78	0.25	12.5
S3 (sub)	623	25	16.5	0.26	68	0.19	12.5
S4 (sup)	673	2	28.2	0.27	53	0.16	14.2
S5 (sup)	673	5	28.0	0.26	47	0.16	16.3
S6 (sup)	673	25	28.4	0.26	37	0.09	19.4
S7 (sup)	723	2	43.4	0.27	40	0.13	19.0
S8 (sup)	723	5	43.8	0.27	37	0.11	19.5
S9 (sup)	723	25	44.3	0.27	39	0.13	20.1
S10 (ss)	1403	5	0.1	0.26	3.2	0.007	42.5
B7 (sup)	723	2	43.4	0	40	0.09	
B10 (ss)	1403	5	0.1	0	0.9	0.004	

[a] *L* is the crystallite size as determined from the Scherrer equation and Ru wt % determined from ICP analysis. (sub) and (sup) refer to subcritical and supercritical hydrothermal conditions, and (ss) refers to solid-state conditions.

K_2CO_3–anatase) and $Na_2O-K_2O-B_2O$ flux[11] or $Li_2O-K_2MoO_4$ flux[12] and the hydrothermal dehydration method from the $TiO_2 \cdot nH_2O-KOH-H_2O$ system[13] were shown to be able to produce long fibers of potassium hexatitanate.

In synthesizing catalytic support materials, generally a method that can produce large surface areas and nanostructure products is desirable. In previous studies, the synthesis of potassium hexatitanate employed for photocatalytic studies [4,8,14–16] so far has been by the solid-state or melt method. Since the hydrothermal synthesis is a powerful route of synthesizing materials,[17–21] this work is directed toward the hydrothermal method of synthesizing potassium hexatitanate. A series of potassium hexatitanates was synthesized under subcritical and supercritical water conditions to determine the optimum preparation conditions for its application as a photocatalyst, using ruthenium oxide as the active phase. As test reaction, water decomposition to hydrogen and oxygen was used due to the increasing importance of hydrogen as a potential source of alternative clean fuel.

Experimental Section

Materials. Potassium hydroxide pellets (Nacalai Tesque Ltd.), titanium tetraisopropoxide (Wako Pure Chemical Industries, Ltd.), potassium carbonate (Kanto Chemical Co. Inc., 99.5%), titanium oxide (anatase, Merck), and ruthenium chloride (Wako Pure Chemical Industries, Ltd., 99.9%) were used as supplied.

Synthesis. Potassium hexatitanates, KTO, were synthesized by hydrothermal reactions by using potassium hydroxide solution and titanium tetraisopropoxide in a K:Ti molar ratio of 1:2. Both reactants were thoroughly stirred for 30 min−1 h before heating in the autoclave using a nickel tube under autogenous pressures. Heating temperatures of 623 K, 16 MPa (subcritical water conditions), 673 K, 28 MPa, and 723 K, 43 MPa (supercritical water conditions), and heating durations of 2, 5, and 25 h were employed. The products were allowed to cool slowly in an autoclave followed by filtering, washing with distilled water and ethanol, and finally drying at 323 K for about 24 h. Synthesis by solid-state reaction was also carried out for comparison using potassium carbonate and titanium oxide (anatase) in a K:Ti molar ratio of 1.1:6 and heating at 1403 K for 5 h. Potassium hexatitanates synthesized by the hydrothermal method were described as ht-KTO, under hydrothermal subcritical and supercritical water conditions as ht-sub-KTO and ht-super-KTO, respectively, and under solid state as ss-KTO.

Loading of Ru on potassium hexatitanates by ion-exchange reaction was carried out using a 0.1 wt % $RuCl_3$ aqueous solution, left overnight at room temperature in a shaker. The solid was filtered, dried at 323 K overnight, and calcined at 623 K for 2 h. The various photocatalysts prepared with the loaded ruthenium oxide on KTO were described as RuO_2/KTO.

Characterization. Elemental contents of the Ru, K, and Ti were analyzed by ICP-ES, Seiko model SPS-1500R. The Ru content was determined from the filtrate after ion-exchange, while Ti and K contents were determined from the solid samples after dissolving them in concentrated sulfuric acid at 353 K. Table 1 shows the Ru wt % loading for the various samples. X-ray diffraction patterns of the as-synthesized samples were recorded on a Rigaku RAD-X system using monochromatized Cu K_α radiation (40 kV, 20 mA, scan speed 2 deg/min) to confirm formation of potassium hexatitanates (JCPDS 40−0403).[22] The surface structure and morphology were studied by scanning electron microscopy (Hitachi S-800) and transmission electron microscopy (JEOL JEM-2000EXII). The surface analysis was performed on XPS (Ulvac PHI ESCA-5600). Thermal analysis was performed using a Rigaku Thermoflex TG-8101D thermogravimetry-differential thermal analyzer (TG-DTA) referenced with recalcined alumina at a ramping rate of 10 K/min in air. UV−vis diffuse reflectance spectra were recorded on a Hitachi-340 spectrophotometer that was equipped with an integrating sphere. Powder samples were loaded in a quartz cell and measurement was taken in a wavelength range of 200−850 nm against a standard. N_2 adsorption measurements were carried out at 77 K with a Micromeritics ASAP 2000 instrument. The samples were degassed at 473 K for about 5 h until the pressure reached <20 mTorr. The volume of adsorbed N_2 was normalized to standard temperature and pressure. The BET surface area was calculated by using the BET equation and the pore size distribution was calculated by using the desorption isotherm and the Barret-Joyner-Halenda (BJH) formula.

(11) Yokoyama, M.; Ota, T.; Yamai, I. *J. Mater. Sci. Lett.* **1994**, *13*, 369.
(12) Yokoyama, M.; Ota, T.; Yamai, I. *J. Mater. Sci.* **1989**, *24*, 3787.
(13) Ota, T.; Saito, H. *J. Cryst. Growth* **1979**, *46* , 331.
(14) Ogura, S.; Kohno, M.; Sato, K.; Inoue, Y. *J. Mater. Chem.* **1998**, *8* (11), 2335.
(15) Ogura, S.; Kohno, M.; Sato, K.; Inoue, Y. *Appl. Surf. Sci.* **1997**, *121/122*, 521.
(16) Inoue, Y.; Asai, Y.; Sato, K. *J. Chem. Soc., Faraday Trans.* **1994**, *90* (5), 797.
(17) Demazeau, G. *J. Mater. Chem.* **1999**, *9*, 15.
(18) Cansell, F.; Chevalier, B.; Demourgues, A.; Etourneau, J.; Even, C.; Garrabos, Y.; Pessey, V.; Petit, S.; Tressaud, T.; Weill, F. *J. Mater. Chem.* **1999**, *9*, 67.
(19) Adshiri, T.; Yamane, S.; Onai, S.; Arai, K. *Supercritical Fluids-Reaction, Material Science and Chromatography, 13*; AIPFS Publishing: Nancy, France, 1994.
(20) Kominami, H.; Matsuura, T.; Iwai, K.; Ohtani, B.; Nishimoto, S.-I.; Kera, Y. *Chem. Lett.* **1995**, 693.
(21) Hakuta, Y.; Seino, K.; Ura, H.; Adsciri, T.; Takizawa, H.; Arai, K. *J. Mater. Chem.* **1999**, *9*, 2671.
(22) Andersen, E. K.; Andersen, I. G. K.; Skou, E. *Solid. State Ionics* **1988**, *27*, 181.

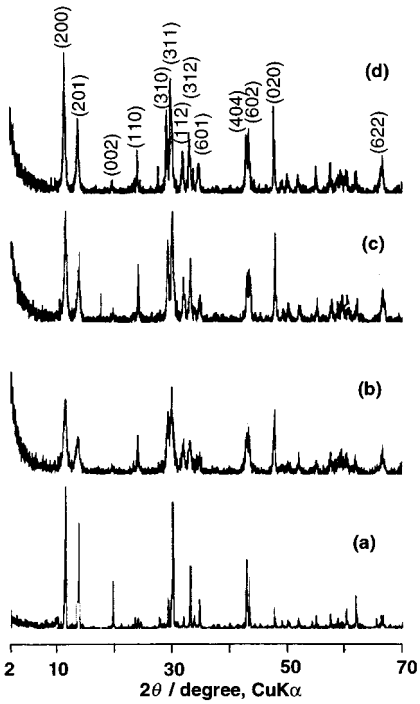

Figure 2. XRD patterns of KTO synthesized at various heating temperatures for a heating duration of 5 h. (a) 1403 K (solid-state method); (b) 623 K; (c) 673 K; (d) 723 K (hydrothermal method).

Photocatalytic Activity. Photocatalytic reaction was carried out in a closed gas-circulation system at 303 K. The catalyst (ca. 0.30 g) placed in the Pyrex glass reactor containing 500 cm^3 distilled water and was kept in suspension by stirring continuously with a magnetic stirrer. Nitrogen gas was passed through the reactor to flush off any dissolved gas residues for about 30 min−1 h before starting the reaction. The UV source was a high-pressure Hg lamp (400 W) placed in a doubled-wall Pyrex glass cooling water circulator in the center of the reactor. A gas chromatograph with an auto-sampler (1 cm^3) and connected directly to the reactor was used to monitor the gas products. The column used consisted of molecular sieve 13X column with argon carrier gas and detection by TCD. Sampling was carried out every 30 min.

Results and Discussion

XRD. Figure 2 shows the XRD patterns of the ht-KTO samples synthesized with a 5-h heating duration under sub- and supercritical water conditions and the ss-KTO sample. Diffraction peaks observed with d(200) ca. 7.69 (2ϑ of 11.5° for the 100% intensity) are in good agreement with those reported[9] for KTO. All the XRD patterns for the ht-KTO are quite similar, though peaks appear slightly sharper for the ht-KTO samples synthesized under supercritical water conditions as compared to those synthesized under subcritical water conditions. However, generally the peak patterns for the ht-KTO samples are not as sharp as those of the ss-KTO sample. The absence of very sharp peaks suggests that the ht-KTO products are not highly crystalline and crystallite sizes are small. Table 1 shows the crystallite size as determined by the Debye−Scherrer equation for the (200) reflection. Crystallite size in the direction of (200) is also about twice as large for the ss-KTO sample (42.5 nm), as compared to the ht-KTO samples (ca. 16.3 ± 3.8 nm). Generally, the ht-KTO samples synthesized under supercritical water conditions tend to be larger than those synthesized under subcritical water conditions. The crystallite size for the ht-KTO samples also seems to increase with heating duration.

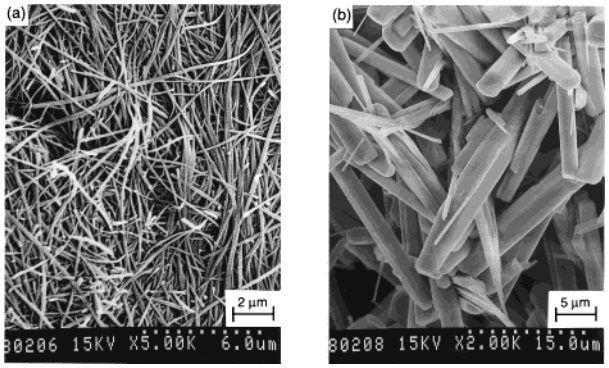

Figure 3. Scanning electron micrographs of potassium hexatitanates as synthesized at a heating duration of 5 h. (a) Hydrothermal condition at 723 K; (b) solid-state condition at 1403 K.

The XRD diffractograms also show that peaks at d(110) and (020) are more intense for the ht-KTO samples than for the ss-KTO sample. Earlier work on electron diffraction studies has shown that KTO fibers synthesized by the dehydration hydrothermal method consisted of crystals grown in the direction of (110).[13] Thus, the more intense peaks at d(110) and d(020) suggest that KTO prepared by the above hydrothermal method produces fibers with crystal growth in the (110) and (020) direction. However, the intensity of the peak at d(002) for the ss-KTO is 6-fold higher than for ht-KTO, suggesting that the crystal growth of the fiber in the direction (002) is more pronounced for the solid-state method as compared to the hydrothermal method, resulting in formation of larger and more crystalline fibers.

Electron Microscopies (SEM and TEM). Figure 3 shows the SEM images of the KTO samples synthesized under hydrothermal condition at 723 K and solid-state condition at 1403 K, respectively. The micrographs of all the ht-KTO samples generally showed similar morphology of long, felt-like fibrous structures, while that of the ss-KTO sample showed short fibers and only few long fibers. Particle size of ss-KTO sample observed was also larger as compared to ht-KTO samples. This is in accord with the results obtained from XRD.

TEM observations revealed that the particulate morphology of ht-KTO samples is long, thin fibers of length >25 nm and diameter ca. 0.5 nm, while the ss-KTO is mainly thick short fibers with few thin long fibers (Figure 4). Electron diffractions from TEM for both ht-KTO and ss-KTO show that the fibers grow along the *b*-axis, i.e., in the (010) direction. The growth of KTO fibers along the *b*-axis is less for the ss-KTO sample compared to the ht-KTO samples as the intensity at d(020) in the XRD diffractogram of the former is less than that of the latter.

To observe the ruthenium oxide, higher loading of 1.1 wt % ruthenium was used. HRTEM showed spherical dark spots which can be attributed to the ruthenium oxide. Larger spots with a diameter ca. 3.5−5.0 nm and uniformly dispersed on the ss-KTO fiber were observed.[15] In the ht-KTO samples these spots tend to be smaller and not easily observed (Figure 5). These results

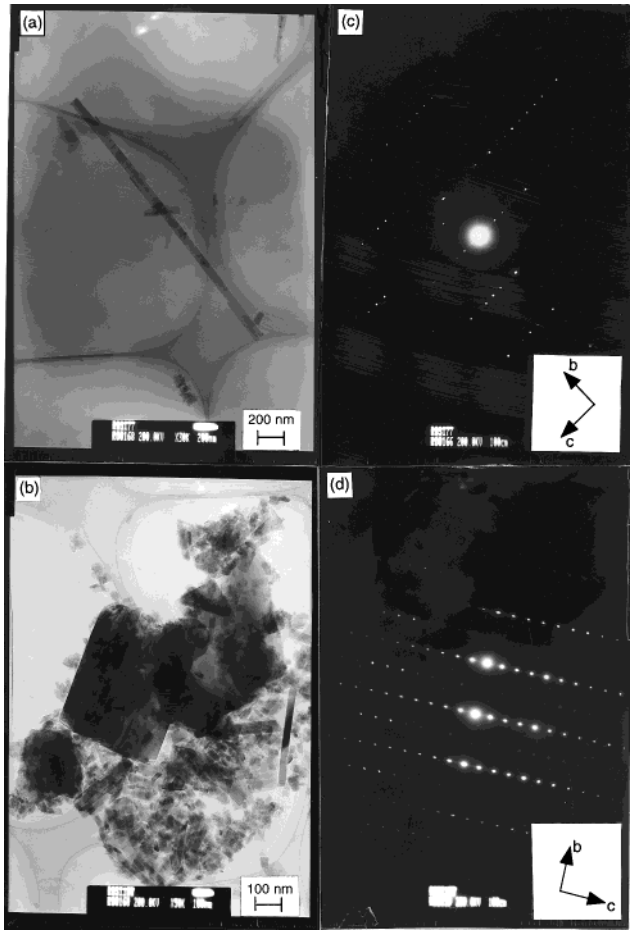

Figure 4. TEM images and electron diffraction patterns of the KTO fibers synthesized under hydrothermal condition at 723 K for 5 h (a, c) and by the solid-state reaction at 1403 K for 5 h (b, d).

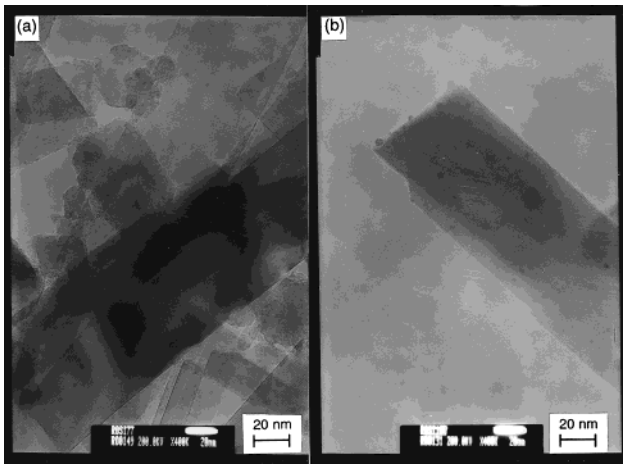

Figure 5. TEM images of Ru oxide on KTO fibers synthesized (a) hydrothermally at 723 K, 2 h, and (b) by solid-state reaction at 1403 K, 5 h.

suggest that the ruthenium oxide might have dispersed more in the inner KTO lattice of the ht-KTO samples.

X-ray Photoelectron Spectra. Surface analysis of the active phase, ruthenium oxide, was done on the 1.1 wt % ruthenium loading. Presence of ruthenium species was detected only in the ss-KTO sample, while no ruthenium species was detected in the ht-KTO samples. Deconvolution of the peaks revealed two types of ruthenium species in a ratio of 60:40 and with binding

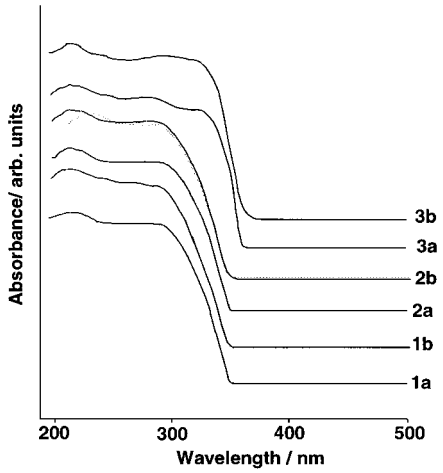

Figure 6. UV−visible diffuse reflectance of KTO with ruthenium oxide (1b, 2b, 3b) and without ruthenium oxide (1a, 2a, 3a). 1 and 2 are KTO samples synthesized hydrothermally at 723 K for 2 and 5 h, respectively, while 3 is a KTO sample prepared by solid-state reaction at 1403 K for 5 h.

energies of Ru $3d_{5/2}$ at 280.8 and 282.6 eV, respectively. The former value can be assigned to RuO_2 and this is in very close agreement with the value of 280.6−280.7 eV obtained in earlier works.[4,23] From ICP results, the ruthenium loading is about the same for both ht-KTO and ss-KTO samples, thus the absence of ruthenium species on the surface of the ht-KTO samples suggests that the ruthenium species might be in the inner KTO lattice. To confirm this, sputtering for 10 min was carried out on the RuO_2/ht-super-KTO samples synthesized at 723 K for 2 h. The results showed ca. 1.3 wt % Ru species were detected, indicating the presence of Ru species in the inner KTO lattice.

Thermal Analysis. No weight loss up to 1273 K was observed by TGA, showing that all the KTO fibers, synthesized either by the hydrothermal or the solid-state method, have good thermal stability. Similarly, no significant thermal effects were observed in the DTA curves, indicating thermal stability and no phase transformation or appreciable hydroxyl groups present.

Diffuse Reflectance UV−Visible Spectra. The diffuse reflectance UV−visible spectra of the calcined ht-KTO and ss-KTO samples with and without ruthenium oxide loading were depicted in Figure 6. The spectra for all the ht-KTO samples show the onset of absorption at ca. 356 nm (ca. 3.48 eV), while for the ss-KTO sample the onset is ca. 360 nm (ca. 3.44 eV) without ruthenium oxide and shift to slightly to ca. 2 nm to higher wavelength with the presence of ruthenium oxide. The above results show that the presence of ruthenium oxide at ca. 0.27 wt % loading generally does not seem to effect the band gap. Absorption of light by the KTO for charge separation can readily occur upon irradiation without any interference from the ruthenium oxide particles.

N_2 Adsorption Measurement. The surface measurement data for the calcined RuO_2/KTO samples are also shown in Table 1. Generally, the surface areas decrease with heating temperatures. Increasing the heating duration seems to affect the surface areas in an increasing order of 2 h > 5 h > 25 h for the RuO_2/

(23) Kim, K. S.; Winograd, N. *J. Catal.* **1974**, *35*, 66.

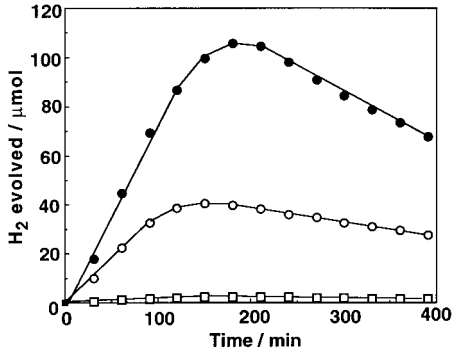

Figure 7. Time course of hydrogen evolution from water decomposition over various Ru oxide/KTO's. (○) ht-sub-KTO (S5); (●) ht-super-KTO (S8); (□) ss-KTO(S10). Reaction conditions: catalyst, 0.3 g; H_2O, 500 cm^3; a high-pressure mercury lamp (400 W); an inner irradiation type Pyrex cell.

ht-sub-KTO samples and the RuO_2/ht-super-KTO samples synthesized at the lower temperature of 673 K, while the surface areas for the RuO_2/ht-super-KTO samples synthesized at the higher temperature of 723 K remain unchanged. The decrease in surface area is less pronounced for RuO_2/ht-sub-KTO samples, i.e., ca. 18% (from 83 m^2/g for the 2 h duration to 68 m^2/g for 25 h), than the RuO_2/ht-super-KTO samples synthesized at a lower temperature of 673 K, i.e., ca. 30% (from 53 m^2/g for the 2 h duration to 37 m^2/g for 25 h). The surface areas obtained for RuO_2/ht-super-KTO samples synthesized at a higher temperature of 723 K, regardless of heating duration, are quite similar to that obtained for RuO_2/ht-super-KTO samples synthesized at the lower temperature of 673 K for 25 h heating duration, i.e., ca. 38 ± 1 m^2/g. Determination of the pore size distribution showed that the average pore size is unchanged as heating temperature and duration increase.

The lower surface areas obtained as heating temperature increases and, in some cases, as heating duration increases indicate formation of larger crystals. Thus, under subcritical conditions, the ht-KTO crystals formed were small, while under supercritical conditions, the ht-KTO crystals are larger. The surface areas of these ht-KTO samples are found to be more than 10 times larger than that of the ss-KTO sample (3.2 m^2/g).

Photocatalytic Activity. Figure 7 shows the time-dependence profiles of hydrogen evolution from water decomposition over various RuO_2/KTO photocatalysts. In all cases, the hydrogen production increases progressively and then decreases with irradiation time. Similar profiles and results were also observed for all the other RuO_2/ht-KTO samples. The decrease of hydrogen production observed after a certain irradiation time somehow differs for each photocatalyst. The decrease is more pronounced for the active photocatalyst, i.e., RuO_2/ht-super-KTO, samples synthesized at 723 K than for the RuO_2/ht-sub-KTO samples, and only a slight decrease is observed for the RuO_2/ss-KTO sample. This decrease could be attributed to the build-up of oxygen gas product as the reaction progresses, causing recombination of the products to form back the water. Similar deactivation due to this back-reaction has also been reported in the case of platinum-loaded titania photocatalysts.[24] All the RuO_2/ht-KTO samples show higher activity and more hydrogen production compared to the RuO_2/ss-KTO sample. Similarly, the RuO_2/ht-super-KTO samples synthesized at 723 K produced more hydrogen and were more active than the RuO_2/ht-sub-KTO samples.

Table 2. Activity for Water Decomposition over the Various RuO_2/KTO Photocatalysts[a]

sample	H_2 evolution rate from H_2O, μmol/h	O_2 evolution rate from H_2O, μmol/h
S1(ht-623-2h)	11	10
S2(ht-623-5h)	19	8
S3(ht-623-25h)	27	9
S4(ht-673-2h)	25	8
S5(ht-673-5h)	21	8
S6(ht-673-25h)	34	10
S7(ht-723-2h)	38	8
S8(ht-723-5h)	47	9
S9(ht-723-25h)	31	7
S10(ss-1403-5h)	0.8	12
B7(ht-723-2h)	0.4	7
B10(ss-1403-5h)	0	8

[a] Catalyst, 0.3 g; H_2O, 500 cm^3; light source, high-pressure mercury lamp (400 W); reaction cell, innner irradiation reaction cell; S:Ru loading, 0.26−0.27 wt %; B:Ru unloaded samples.

The hydrogen evolution rate of the various photocatalysts calculated from the initial rate until hydrogen production started to decrease are shown in Table 2, together with oxygen evolution rate. There is no significant difference in the oxygen evolution rate in the photocatalysts examined. The hydrogen evolution rate for water decomposition over the RuO_2/ss-KTO sample (2.7μmol/hg) was comparable to the value previously reported (4.8μmol/hg).[15] The hydrogen evolution rates were remarkably higher for the RuO_2/ht-KTO samples than the RuO_2/ss-KTO sample. The increase in hydrogen evolution rate is ca. 13−34-fold higher for the RuO_2/ht-sub-KTO samples and ca. 26−59-fold higher for the RuO_2/ht-super-KTO samples. Compared with photocatalytic activities for pure water decomposition over other photocatalysts prepared by the solid-state reaction, the maximal hydrogen evolution rate for RuO_2/ht-KTO (157 μmol/hg) is higher than those for RuO_2/$Na_2Ti_6O_{13}$ (29 μmol/hg)[4] and NiO/$K_4Nb_6O_{17}$ (77 μmol/hg).[5] Activity measurements were also carried out on the KTO without the active phase, ruthenium oxide. As shown in Table 2, the ht-KTO sample exhibited very low and insignificant activity, while no activity was observed at all for the ss-KTO sample. This suggests the importance of the presence of ruthenium oxide in promoting water decomposition. Holes produced in the valence band of the TiO_2 photocatalyst are known to oxidize water, even in the absence of RuO_2, while the rate of the process is relatively low.[25] The role of RuO_2 in the water decomposition is to accelerate the hole transfer from the valence band of TiO_2 to the water.[26,27] Ogura et al. demonstrated that ruthenium oxide promotes the efficiency of photoexcited charge transfer from the alkali-metal hexatitanates to the adsorbed reactant.[14] As absorption of UV light for the separation of these photoexcited charges was not hindered by the

(24) Tabata, S.; Nishida, H.; Masaki, Y.; Tabata, K. *Catal. Lett.* **1995**, *34*, 245.
(25) Rao, M. V.; Rajeshwar, K.; Verneker, V. R. Pai; DuBow, J. *J. Phys. Chem.* **1980**, *84*, 1987.
(26) Duonghong, D.; Borgarello, E.; Grätzel, M. *J. Am. Chem. Soc.* **1981**, *103*, 4685.
(27) Borgarello, E.; Kiwi, J.; Pelizzetti, E.; Visca, M.; Grätzel, M. *J. Am. Chem. Soc.* **1981**, *103*, 6324.

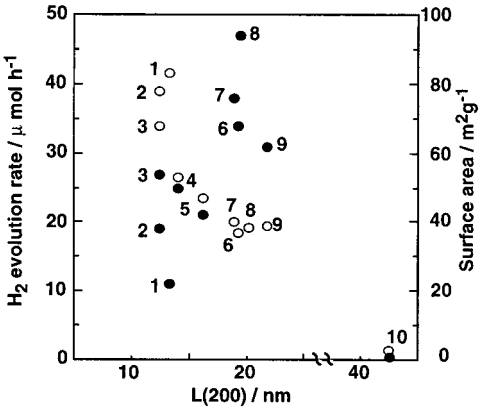

Figure 8. Relationships between photocatalytic activity or surface area and crystallite size of the various Ru oxide/KTO's. The surface area and the hydrogen evolution rate are plotted by open and filled circles, respectively. 1−3 and 4−9 represent KTO synthesized under subcritical and supercritical water conditions, respectively, 10 represents KTO synthesized by solid-state reaction.

presence of these ruthenium oxides (as shown from the UV−visible diffuse reflectance results), the photoexcited electron formed can readily be transferred through the ruthenium oxide for the reduction of the reactant H^+ into hydrogen.

The RuO_2/ht-KTO sample having higher surface area and smaller crystals than the RuO_2/ss-KTO sample is expected to have better dispersion of ruthenium oxide. The higher dispersion of ruthenium oxide will increase the efficiency of photoexcited charge separation and transfer to the surface reactants, thus giving rise to the higher activity as shown in Table 2. The slight activity shown by the ht-KTO sample can also be explained along these lines. The ht-KTO samples, having smaller crystallite size, are able to undergo photoexcited charge separation but slow charge transfer to the surface due to the absence of a promoter. In the larger and low surface area crystals of the ss-KTO sample, the photoexcited charges generated might have recombined in the KTO and the transfer of charge to the surface through the ruthenium oxide might not have taken place at all. How these ruthenium oxides are dispersed on the KTO fibers has yet to be studied, although it has been reported that the ruthenium oxide loaded on supports with tunnel structure could be dispersed both on the surface and in the tunnels.[4]

Figure 8 shows the relationship between photocatalytic activity and crystallite size along the (200) index, together with the surface area of the various RuO_2/KTO photocatalysts. The RuO_2/ht-KTO photocatalysts can be categorized into two groups, those having surface area of ca. 38 ± 1 m^2/g have higher activity, ca. 39 times higher, while those having surface area higher than this value tend to have lower activity, ca. 13 times higher compared to the RuO_2/ss-KTO photocatalyst. It appears that activity is higher for lower surface area RuO_2/ht-KTO samples, which is usually contrary to catalytic performance. The crystallinity of the KTO to a certain extent is beneficial for the photocatalytic activity. The XRD diffractograms show that these lower surface areas ht-super-KTO samples have better crystallinity than the ht-sub-KTO samples. Crystallite size of about 20 nm seems to be the optimum crystallite size for good activity, while too a small crystallite size will tend to lose its crystallinity and thus lower activity. Generally amorphous or poor crystalline phases exhibits lower photocatalytic activity than is exhibited by the crystalline phase.[28] Although there were no impurities in the ht-sub-KTO as shown in the XRD results, defects were considered to exist, which might act as recombination centers for photogenerated electron−hole pairs. As for the ss-KTO sample, though the crystallinity is high as seen from XRD, its surface area is too low for good activity performance. Furthermore, the crystallite size of ss-KTO is too large and this might have prevented the photocatalysts to remain very much in suspension during the reaction.

Conclusions

Different preparative methods have important effects on the resulting microstructure and physical properties of the materials. KTO synthesized hydrothermally under sub- and supercritical water conditions produce thermally stable long, felt-like, thin fibers of large surface area as compared to the short, thick fibers in the solid-state method. The growth of these long fibrous crystals is more pronounced along the *b*-axis (020). The heating temperature and duration employed in the hydrothermal synthesis do not seem to have much effect on the crystal morphology and structure of the KTO products, but they do affect the surface areas and crystallite size of the KTO products. Under subcritical water conditions, the crystals formed were small, while under supercritical conditions, the crystals are larger.

The photocatalytic activities for the water decomposition over RuO_2/ht-KTO are remarkably higher than those over RuO_2/ss-KTO photocatalysts. RuO_2/ht-super-KTO also exhibited higher activity than the RuO_2/ht-sub-KTO photocatalysts. The crystallinity of the photocatalysts seems beneficial to a certain extent for this high photocatalytic activity. The photocatalysts with optimum crystallite size of about 20 nm and surface area of ca. 38 m^2/g seem to have much higher activity.

In summary, this study has exhibited the advantage of the hydrothermal synthesis to prepare a highly active photocatalyst compared with the conventional solid-state reaction.

Acknowledgment. This work has been supported by CREST of JST (Japan Science and Technology) and JICA (Japan International Corporation Agency). We express appreciation to Dr. M. Chatterjee and Dr. A. Chatterjee for their technical help and useful discussion.

CM000561P

(28) Ooka, C.; Akita, S.; Ohashi, Y.; Horiuchi, T.; Suzuki, K.; Komai, S.; Yoshida H.; Hattori, T. *J. Mater. Chem.* **1999**, *9*, 2943.